Characterization of ionospheric disturbances and their relation to GNSS positioning errors at high latitudes

Knut Stanley Jacobsen*and Michael Dähnn
Norwegian Mapping Authority, Norway

Abstract

We present results from an analysis of the distribution of ionospheric disturbances, measured by the Rate Of TEC Index (ROTI), and their relation to Precise Point Positioning (PPP) accuracy. The analysis is based on data for the entire year of 2012, for 10 receivers at latitudes from 59 to 79 degrees North. PPP solutions were computed using the GIPSY software.

The results show that elevated ROTI values occurs mainly in the cusp and nightside auroral oval regions. Elevated ROTI values are more common in the cusp, but in the nightside auroral oval they are stronger. The 3D position error is strongly correlated with ROTI for receivers that are affected by space weather, and increases exponentially with increasing ROTI.

1 Introduction

Global Navigation Satellite System (GNSS) positioning can suffer from a number of different error sources. During strong ionospheric activity, the ionosphere is the dominant error source for GNSS signals.

The occurrence of scintillation at high latitudes is related to the auroral oval, cusp, and polar-cap patches, through the formation of small-scale plasma structures due to particle precipitation or plasma instabilities [e.g. 1, 7, 10, 20, 16, 19, 2, 8, 5, 17, 15]. It has been observed that phase scintillation occurs more often than amplitude scintillation at high latitudes, and that scintillation is more common on geomagnetically disturbed days in the auroral oval region and close to noon and midnight [17, 15, 11, 14, 19, 2].

The Norwegian Mapping Authority (NMA) operates a national network of GNSS receivers, which is used for positioning services and various studies. In this paper, we investigate the link between Precise Point Positioning (PPP) errors and the Rate Of TEC Index (ROTI), which is a commonly used measure of ionospheric activity (see Section 2.2). We also investigate the location of the elevated ROTI values in geomagnetic coordinates, and the probability of having multiple satellites affected simultaneously.

Please note that the contents of this paper is largely based on the work published in *Jacobsen, Knut Stanley and Dähnn, Michael* [6]. That paper contains more information, results and details than what is included in this paper. Any reference to this work should cite that paper.

2 Data sources

This study is based on GNSS data from 10 receivers (see Section 2.1) for the whole year of 2012. The data has been processed to calculate ROTI (see Section 2.2) and PPP coordinates (see section 2.3) at 5 minute resolution.

*knut.stanley.jacobsen@kartverket.no

Table 1: List of receivers

ID	Location	Latitude	Longitude	Receiver Type	Antenna Type
NYAL	Ny-Ålesund	78.93	11.87	Trimble NetRS	AOAD/M_B
NYA1	Ny-Ålesund	78.93	11.87	Trimble NetR8	ASH701073.1
LYRS	Longyearbyen	78.23	15.40	Trimble NetR9	TRM41249.00
HAMC	Hammerfest	70.67	23.66	Trimble NetR5	TRM55971.00
TRO1	Tromsø	69.66	18.94	Trimble NetR8	TRM59800.00
VEGS	Vega	65.67	11.97	Trimble NetR8	TRM59800.00
FOLC	Folling	64.12	11.62	Trimble NetR5	TRM59800.00
HFS4	Hønefoss	60.14	10.24	Trimble NetR5	TRM59800.00
OPEC	Opera	59.91	10.75	Trimble NetR5	TRM55971.00
STAS	Stavanger	59.02	5.60	Trimble NetR8	TRM55971.00

2.1 Receivers

Table 1 lists the basic information of the receivers used in this study. All the receivers are owned and operated by NMA. The receivers run with a sample rate of 1 Hz.

2.2 ROTI

In this study, ionospheric disturbances are measured by the Rate of TEC Index (ROTI) [13]. It characterizes small-scale and/or rapid variations of TEC, and is strongly related to scintillation [3]. Its main advantage over scintillation indices is that it is calculated based on measurements from standard dual-frequency GNSS receivers sampling at 1 Hz, which have been and still are far more common than scintillation receivers.

The equation to calculate ROTI may be found in *Jacobsen, Knut Stanley and Dähnn, Michael* [6]. In this study, the ROTI values are based on 1 Hz measurements, and calculated for time intervals of 5 minutes. An elevation cutoff of 5 degrees was used. Note that for the results presented in Section 3.2, an elevation cutoff of 30 degrees was applied.

2.3 PPP

Precise Point Positioning (PPP) is a processing strategy for GNSS observations that enables the efficient computation of high-quality coordinates, utilizing undifferenced dual-frequency code and phase observations by using precise satellite orbit and clock products. More detailed descriptions of PPP can be found in e.g. *Zumberge et al.* [21] and *Kouba and Héroux* [9].

Previous studies by *Tiwari et al.* [18] and *Moreno et al.* [12] have examined the effects of ionospheric disturbances on PPP calculations at low/equatorial latitudes. *Moreno et al.* [12] concluded that the presence of large ROT can induce a significant degradation of the position estimation.

To study how a disturbed ionosphere affects the PPP calculations, we have used the GIPSY software provided by NASAs Jet Propulsion Laboratory (JPL) to compute coordinates for the receivers listed in Table 1. The coordinates were computed with a time resolution of 5 minutes. Important parameters/models used for the GIPSY PPP solutions are summarized in Table 2.

Table 2: Parameters/models used for the GIPSY PPP solution

GIPSY version:	6.1.2
Reference frame:	IGS08/IGb08
Elevation Angle Cutoff:	10 degree
Antenna phase center (receivers):	Absolute based on IGS standard e.g. igs08_1645.atx
Antenna phase center (transmitters):	Absolute based on IGS standard e.g. igs08_1645.atx
Troposphere mapping function:	VMF1
2nd order ionosphere model:	Not applied
Ocean loading:	FES2004
Ambiguity resolution:	Yes [4]

3 Observations

3.1 ROTI vs. PPP error

To investigate the link between ROTI and PPP positioning error, we calculated the mean ROTI across all observed satellites for every 5 minutes, at the times corresponding to the PPP solutions.

The long-term trend was removed from the PPP solutions by subtracting a linear fit to the coordinate time series for the entire year, for each receiver. The 3D position error (P_{3D}) was then defined as the offset of the detrended coordinate from its median value (x_0, y_0, z_0) and calculated for each epoch i as:

$$P_{3D}(i) = \sqrt{(x(i) - x_0)^2 + (y(i) - y_0)^2 + (z(i) - z_0)^2} \tag{1}$$

Then, for each receiver and each hour we calculated the mean ROTI ($\overline{ROTI_{1h}}$) and the standard deviation of P_{3D} (σ_{3D_1h}). These hourly resolution values were then correlated, for an exponential relationship:

$$\sigma_{3D\_1h} = a \cdot e^{(b \cdot \overline{ROTI_{1h}})} \tag{2}$$

where a and b are the parameters of the fit.

Details of the fitting results can be found in *Jacobsen, Knut Stanley and Dähnn, Michael* [6].

To further distill the data, we binned the hourly 3D position errors by the hourly ROTI value in intervals of 0.5 TECU/min and computed the mean and standard deviation of the 3D position errors within each bin. Results from the 6 northernmost receivers are presented in Figure 1. Note that results are not calculated, and thus not shown in the figures, for bins that contain less than 10 samples.

3.2 ROTI occurrence statistics

To avoid the elevation dependency of ROTI values, we used an elevation cutoff of 30 degrees for the analysis of ROTI occurrence. The ROTI data were binned by magnetic latitude (MLAT) and magnetic local time (MLT), at a resolution of 1 degree and 1 hour. Most bins have between 1000 and 10000 samples, which is a good amount of samples for a statistical analysis. Unfortunately, there is no data coverage at latitudes above 80 degrees. This is due to the combination of inclined satellite orbits, the use of an elevation cutoff, and the general lack of receivers around the North Pole.

Figure 2a shows the mean ROTI for all the data from 2012, Figure 2b shows the percentage of observations which had a ROTI greater than or equal to 3.5 TECU/min, and Figure 2c shows the percentage of observations which had a ROTI greater than or equal to 5 TECU/min.

3.3 ROTI risk

Figure 3 contain tables showing the probability to have certain levels of ROTI simultaneously affecting several satellites observed by the same receiver, for the 6 northernmost receivers. For each entry (colored square) in the figures, the probability was calculated simply as the percentage of ROTI measurement epochs (5 minute resolution) in which the ROTI values simultaneously exceeded the defined level for the given number of satellites. The data set covers the entire year of 2012. As an example of how to read the tables, in Figure 3, panel B, the probability of simultaneously having 2 satellites at a ROTI value of at least 3 TECU/min, is around 2 %.

4 Discussion

The statistical analysis in Section 3.1 shows the connection between ROTI and PPP positioning errors. While the three receivers at the lowest latitudes (59^o - 60^o North) show little to no correlation, the receivers at higher latitudes (64^o - 79^o North) show a strong positive correlation (0.4 to 0.7). The best correlation is exhibited by the receivers TRO1 and HAMC, located at about 70^o North. The missing correlation at low latitude receivers can be explained by the lack of strong ionospheric activity in those regions. Only strong events move the auroral oval far enough south to affect these receivers.

Figure 1 shows the statistical connection between ROTI and positioning error. The position error increases exponentially as a function of ROTI for all receivers except NYAL. For NYAL, it increases faster than exponentially. It is not clear why this is so, but we note that NYAL is the only site with a NetRS receiver (see Table 1), which is the oldest type of receiver amongst those used in this study. The receiver NYA1, which is colocated with NYAL, has an entirely different result that is more in line with the other receivers. It is plausible that the processing in the NetRS receiver is more vulnerable to noisy measurements than the newer generations of receivers.

In Section 3.2 results regarding the location of elevated ROTI values in a geomagnetic reference frame (MLAT & MLT) were presented. The mean ROTI (Fig. 2a) is elevated above 70^o North on the dayside, and above 60^o North on the nightside. Two regions have especially elevated values; The post-noon sector (12 to 16 MLT) at around 75^o-80^o North on the dayside, and the region around midnight (22 to 02 MLT) at around 70^o North on the nightside. These regions correspond to the cusp region and the nightside auroral oval. The asymmetry observed for the ROTI distribution in the cusp region could be caused by an asymmetry in the values of the interplanetary magnetic field Y-component for the geomagnetic storms that occurred during 2012.

These regions are also found in the plots of occurrence of strong (>= 3.5 TECU/min) and very strong (>= 5 TECU/min) ROTI (Figs. 2b and 2c). It is interesting to note that in the plot of strong ROTI, the occurrence is greater in the cusp region than at the nightside, but in the plot of very strong ROTI, the occurrence is much stronger in the nightside auroral oval region. This means that elevated ROTI values are more common in the cusp region, but when they occur in the nightside auroral oval region they are stronger than in the cusp.

In Section 3.3 tables showing the risk of simultaneously having several satellites with high ROTI values were presented. Generally, both the magnitude of ROTI, and the number of satellites affected, were higher for receivers at higher latitudes. For the northernmost receivers (Fig. 3, panels A, B and C), which are located at Svalbard, the maximum number of simultaneously affected satellites at high ROTI levels was somewhat less than that for receivers in the middle of Norway. This is caused by less satellites being visible at such a high latitude. Whether these risks are significant or not, depends on the kind of system that uses the data, and what thresholds are set for that system.

We note that *Aquino et al.* [2] has made similar risk statistics for phase scintillation observed at Hammerfest, based on data from 2002-2003. The general pattern is the same as we see for ROTI at the same location (see Fig. 3, panel D), but with far lower probabilities.

5 Conclusions

- For receivers that experienced strong space weather effects (Located above 64^o North), there is a strong positive correlation between PPP error and ROTI. The 3D position error increases exponentially with increasing ROTI.
- Elevated ROTI values occur mainly in the cusp region and in the nightside auroral oval. It most commonly occurs in the cusp region, but when it occurs in the nightside auroral oval, it is stronger.
- The risk of having several satellites observing enhanced ROTI values simultaneously is greater at higher latitudes. We have presented tables of the risks for receivers at different latitudes in Norway (Fig. 3).

6 Acknowledgements

This paper is based on the work published in *Jacobsen, Knut Stanley and Dähnn, Michael* [6]. MLAT and MLT were computed using the Altitude Adjusted Corrected Geomagnetic Coordinate (AACGM) software. PPP solutions were computed using the GIPSY software, developed by NASA/JPL.

References

[1] Aarons, J. (1997), Global positioning system phase fluctuations at auroral latitudes, *Journal of Geophysical Research: Space Physics*, *102*(A8), 17,219–17,231, doi:10.1029/97JA01118.

[2] Aquino, M., F. S. Rodrigues, J. Souter, T. Moore, A. Dodson, and S. Waugh (2005), Ionospheric scintillation and impact on gnss users in northern europe: Results of a 3 year study, *Space Communications*, *20*(1-2), 17–29.

[3] Basu, S., K. Groves, J. Quinn, and P. Doherty (1999), A comparison of {TEC} fluctuations and scintillations at ascension island, *Journal of Atmospheric and Solar-Terrestrial Physics*, *61*(16), 1219 – 1226, doi:http://dx.doi.org/10.1016/S1364-6826(99)00052-8.

[4] Bertiger, W., S. D. Desai, B. Haines, N. Harvey, A. W. Moore, S. Owen, and J. P. Weiss (2010), Single receiver phase ambiguity resolution with gps data, *Journal of Geodesy*, *84*(5), 327–337, doi: 10.1007/s00190-010-0371-9.

[5] Burston, R., I. Astin, C. Mitchell, L. Alfonsi, T. Pedersen, and S. Skone (2010), Turbulent times in the northern polar ionosphere?, *Journal of Geophysical Research: Space Physics*, *115*(A4), doi: 10.1029/2009JA014813.

[6] Jacobsen, Knut Stanley, and Dähnn, Michael (2014), Statistics of ionospheric disturbances and their correlation with gnss positioning errors at high latitudes, *J. Space Weather Space Clim.*, *4*, A27, doi:10.1051/swsc/2014024.

[7] Kersley, L., C. D. Russell, and D. L. Rice (1995), Phase scintillation and irregularities in the northern polar ionosphere, *Radio Science*, *30*(3), 619–629, doi:10.1029/94RS03175.

[8] Kivanc, Ö., and R. A. Heelis (1997), Structures in ionospheric number density and velocity associated with polar cap ionization patches, *Journal of Geophysical Research: Space Physics*, *102*(A1), 307–318, doi:10.1029/96JA03141.

[9] Kouba, J., and P. Héroux (2001), Precise point positioning using igs orbit and clock products, *GPS Solutions*, *5*(2), 12–28, doi:10.1007/PL00012883.

[10] Krankowski, A., I. Shagimuratov, L. Baran, I. Ephishov, and N. Tepenitzyna (2006), The occurrence of polar cap patches in {TEC} fluctuations detected using {GPS} measurements in southern hemisphere, *Advances in Space Research*, *38*(11), 2601 – 2609, doi:http://dx.doi.org/10.1016/j.asr.2005.12.006, middle and Upper Atmospheres, Active Experiments, and Dusty Plasmas.

[11] Moen, Jøran, Oksavik, Kjellmar, Alfonsi, Lucilla, Daabakk, Yvonne, Romano, Vineenzo, and Spogli, Luca (2013), Space weather challenges of the polar cap ionosphere, *Journal of Space Weather and Space Climate*, *3*, A02, doi:10.1051/swsc/2013025.

[12] Moreno, B., S. Radicella, M. C. Lacy, M. Herraiz, and G. Rodriguez-Caderot (2011), On the effects of the ionospheric disturbances on precise point positioning at equatorial latitudes, *GPS Solutions*, *15*(4), 381–390, doi:10.1007/s10291-010-0197-1.

[13] Pi, X., A. J. Mannucci, U. J. Lindqwister, and C. M. Ho (1997), Monitoring of global ionospheric irregularities using the worldwide gps network, *Geophysical Research Letters*, *24*(18), 2283–2286, doi:10.1029/97GL02273.

[14] Prikryl, P., P. T. Jayachandran, S. C. Mushini, D. Pokhotelov, J. W. MacDougall, E. Donovan, E. Spanswick, and J.-P. St.-Maurice (2010), Gps tec, scintillation and cycle slips observed at high latitudes during solar minimum, *Annales Geophysicae*, *28*(6), 1307–1316, doi:10.5194/angeo-28-1307-2010.

[15] Prikryl, P., R. Ghoddousi-Fard, B. S. R. Kunduri, E. G. Thomas, A. J. Coster, P. T. Jayachandran, E. Spanswick, and D. W. Danskin (2013), Gps phase scintillation and proxy index at high latitudes during a moderate geomagnetic storm, *Annales Geophysicae*, *31*(5), 805–816, doi:10.5194/angeo-31-805-2013.

[16] Skone, S., M. Feng, R. Tiwari, and A. Coster (2009), "characterizing ionospheric irregularities for auroral scintillations", in *Proceedings of the 22nd International Technical Meeting of The Satellite Division of the Institute of Navigation (ION GNSS 2009)*, pp. 2551–2558, Savannah, GA.

[17] Spogli, L., L. Alfonsi, G. De Franceschi, V. Romano, M. H. O. Aquino, and A. Dodson (2009), Climatology of gps ionospheric scintillations over high and mid-latitude european regions, *Annales Geophysicae*, *27*(9), 3429–3437, doi:10.5194/angeo-27-3429-2009.

[18] Tiwari, R., S. Bhattacharya, P. K. Purohit, and A. K. Gwal (2009), Effect of tec variation on gps precise point at low latitude, *The Open Atmospheric Science Journal*, *3*, 1–12, doi:10.2174/1874282300903010001.

[19] Tiwari, R., F. Ghafoori, O. Al-Fanek, O. Haddad, and S. Skone (2010), "investigation of high latitude ionospheric scintillations observed in the canadian region", in *Proceedings of the 23rd International Technical Meeting of The Satellite Division of the Institute of Navigation (ION GNSS 2010)*, pp. 349–360, Portland, OR.

[20] Weber, E. J., J. A. Klobuchar, J. Buchau, H. C. Carlson, R. C. Livingston, O. de la Beaujardiere, M. McCready, J. G. Moore, and G. J. Bishop (1986), Polar cap f layer patches: Structure and dynamics, *Journal of Geophysical Research: Space Physics*, *91*(A11), 12,121–12,129, doi:10.1029/JA091iA11p12121.

[21] Zumberge, J. F., M. B. Heflin, D. C. Jefferson, M. M. Watkins, and F. H. Webb (1997), Precise point positioning for the efficient and robust analysis of gps data from large networks, *Journal of Geophysical Research: Solid Earth*, *102*(B3), 5005–5017, doi:10.1029/96JB03860.

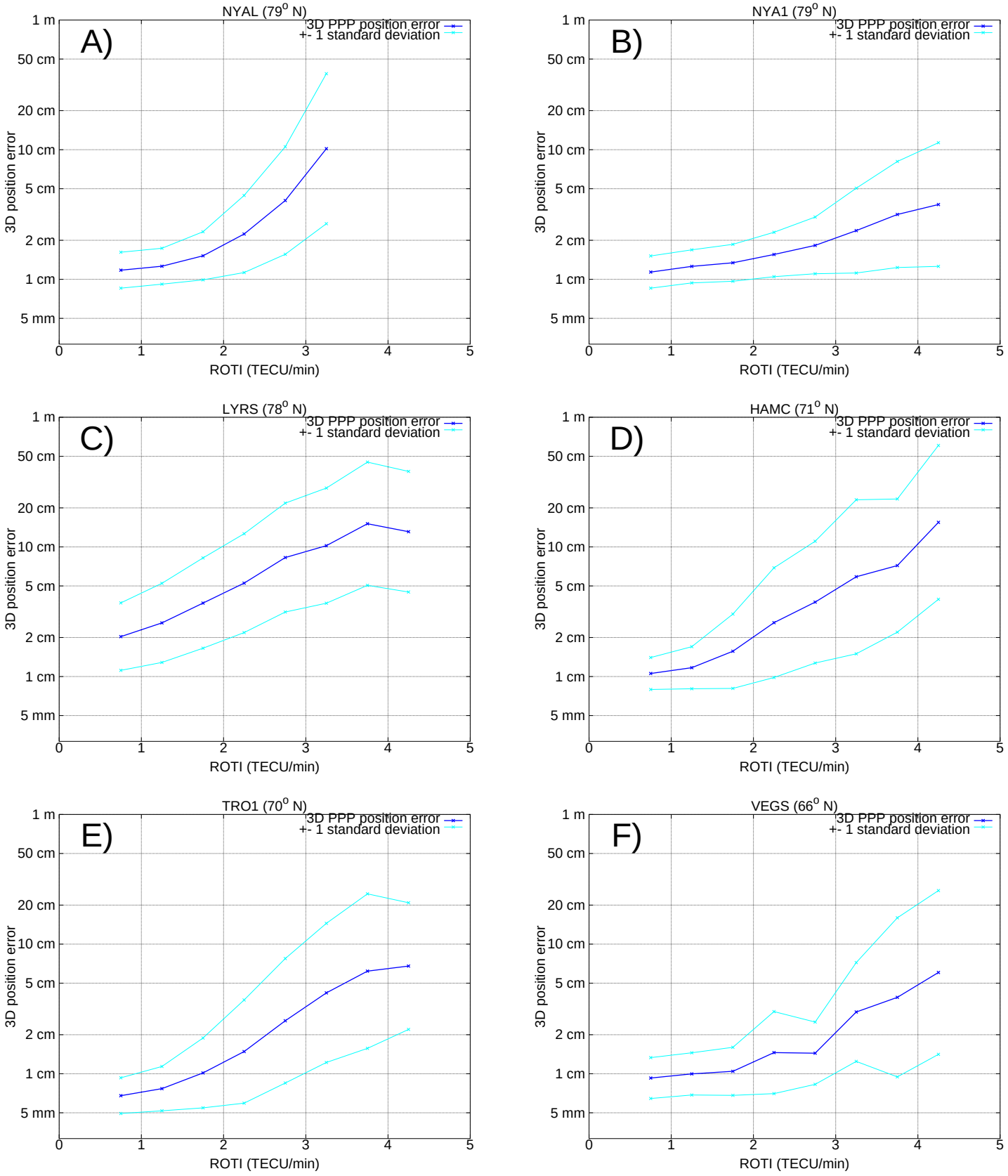

Figure 1: Statistical relationship between mean ROTI and 3D position error, for these receivers: **A**) NYAL **B**) NYA1 **C**) LYRS **D**) HAMC **E**) TRO1 **F**) VEGS

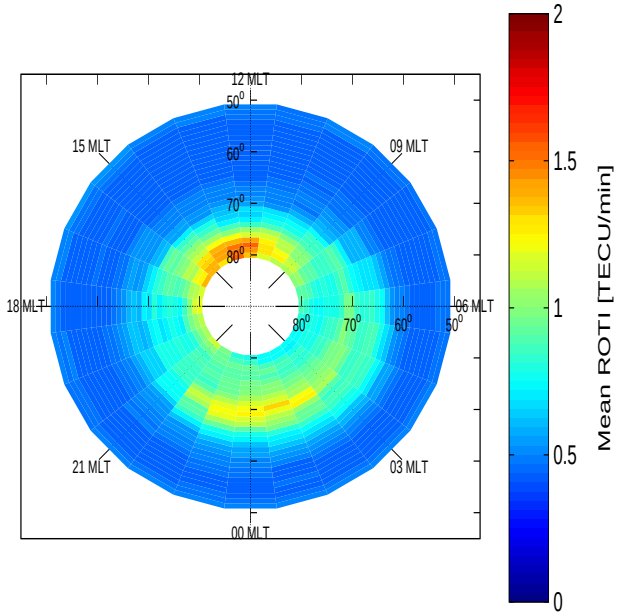

(a) Mean ROTI for 2012, with an elevation cutoff of 30^o.

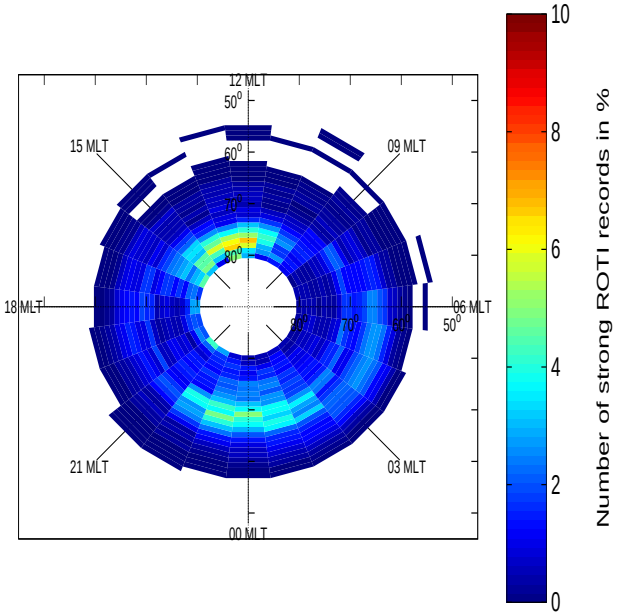

(b) Number of ROTI >= 3.5 TECU/min in percent, with an elevation cutoff of 30^o.

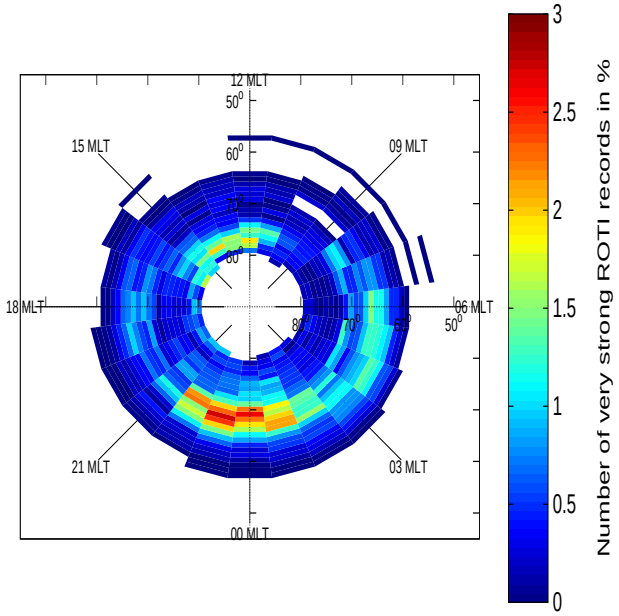

(c) Number of ROTI >= 5 TECU/min in percent, with an elevation cutoff of 30^o. Note that the color scale is different from the color scale in Fig. 2b.

Figure 2: ROTI value statistics for the year 2012, plotted as a function of magnetic latitude and magnetic local time.

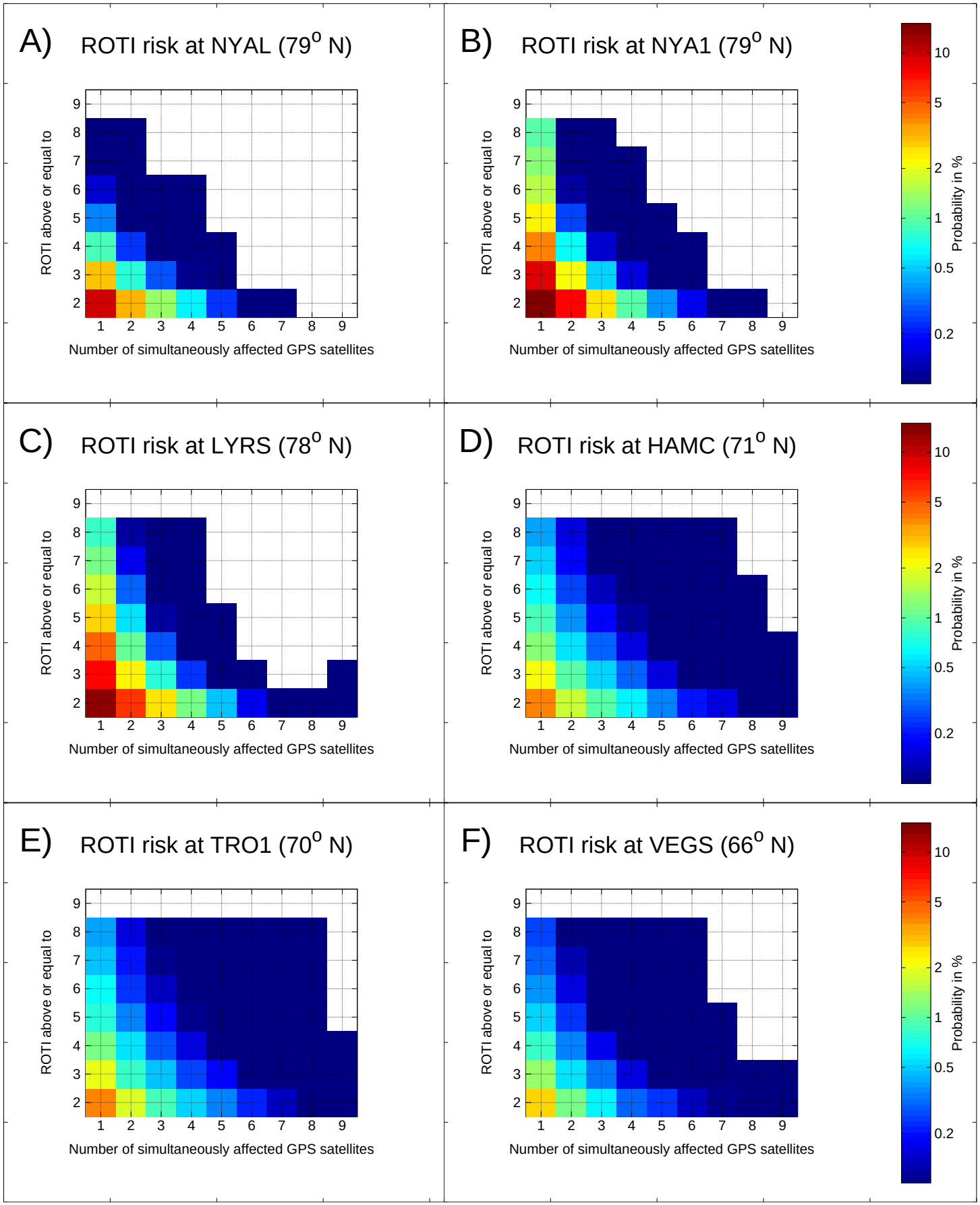

Figure 3: Tables of the probabilities that ROTI exceeds threshold values simultaneously at several satellites, for these receivers: **A**) NYAL **B**) NYA1 **C**) LYRS **D**) HAMC **E**) TRO1 **F**) VEGS